

INTEGRATED INSAR AND GPS STUDIES OF CRUSTAL DEFORMATION IN THE WESTERN GREAT BASIN, WESTERN UNITED STATES

W.C. Hammond^{*a}, Z. Li^b, H.-P. Plag^a, C. Kreemer^a, G. Blewitt^a

^a Nevada Geodetic Laboratory, Nevada Bureau of Mines and Geology, University of Nevada, Reno, Reno, NV, 89557-0178, USA - (whammond, hpplag)^{@unr.edu}

^b Department of Geographical and Earth Science, University of Glasgow, Glasgow, G12 8QQ UK - Zhenhong.Li^{@ges.gla.ac.uk}

KEY WORDS: InSAR, GPS, crustal deformation, Yucca Mountain, vertical motion, reference frame

ABSTRACT:

We compare the level of precision obtainable from GPS and InSAR measurements of the patterns and rates of crustal deformation in the western Great Basin, western United States. In principal InSAR measurements can provide improved geographic resolution of geodetic coverage, complementing GPS networks which are limited by their station spacing. We select the Yucca Mountain, Nevada region as a test case because of its relatively dense coverage with long-running high-quality GPS stations (generally >10 years of data), and its long history of ERS and ENVISAT radar acquisitions (>17 years of data). We apply a time series algorithm to the interferograms in order to estimate linear rates of motion at each pixel, and then adjust the resulting satellite line-of-sight (LOS) rate map to conform to GPS estimates of LOS rate. This aligns the InSAR LOS motion estimates to the GPS reference frame. The resulting LOS deformation map agrees with GPS measurements to within 0.35 mm/yr RMS misfit at the stations and 0.35 mm/yr RMS misfit to the strain map obtained from the GPS velocities. This level of precision is nearly as good as the misfit between GPS velocities and the velocity interpolation (strain map), and represents a considerable improvement over some recent published studies using integrated InSAR and GPS methods. This suggests that the uncertainty in radar LOS rate maps can be brought below 0.35 mm/yr, and that LOS rate maps obtained from InSAR measurements may in future be able to provide a suitable alternative to interpolation of GPS rates which is commonly done in the production of GPS strain maps. The increasing availability of InSAR from satellites such as PALSAR and the future DESDynI will make this approach a valuable tool for hazardous areas.

1. INTRODUCTION

Improving our knowledge of crustal deformation patterns and rates is central to improving our understanding of dynamic processes at work in the continental lithosphere, and to quantifying seismic and other geohazard. To this end, we are developing maps of long term background crustal deformation in the western Great Basin, western United States, using integrated InSAR and GPS data. These products are needed to build better maps of seismic hazard for the growing communities of Reno and Las Vegas, Nevada. Earlier geologic and geodetic studies have shown that the deformation field is complex, with hundreds of fault segments accommodating progressive transensional strain of the crust (e.g. Bennett et al., 2003; Wesnousky, 2005; Hammond et al., 2007). While regional high-precision GPS networks have ~20 km geographic spacing, and are precise enough to resolve the background deformation (~10 mm/yr over ~100 km), InSAR is being explored as a tool to increase the density of geodetic observations of long-term interseismic deformation (e.g. Fialko, 2006; Zebker et al., 2010). Increasing the density of observations should allow us to 1) detect or rule out the existence of shorter wavelength deformation features (such as fault creep) which can affect strain accumulation rates of faults, and 2) measure interseismic vertical motions which can improve constraints on subsurface fault geometry.

New progress in this area is possible because of the increased amount of GPS and InSAR data available and because of improved analysis techniques. New GPS networks in the western Great Basin, including the EarthScope "Plate Boundary Observatory" (<http://www.earthscope.org>) and our own "MAGNET" (Mobile Array of GPS for Nevada Transtension, <http://geodesy.unr.edu/networks>, Blewitt et al., 2009), provide better station coverage than was previously available. Also GPS time series have lengthened, averaging out stochastic

noise, seasonal variations, and small non-secular transients, and thus improve estimates of interseismic deformation rate. For InSAR, acquisition of large numbers of radar scenes provides longer temporal baselines and a greater number of opportunities to form interferometric pairs with shorter geometric baselines which improve coherence.

Since GPS and InSAR are both sensitive to motions of the Earth surface, they should be capable of measuring the same signals, and should agree where both measurements are available. It is well known, however, that InSAR measurements suffer from the presence of atmospheric water vapor which introduces artifacts to the imagery. GPS solutions however correct for water vapor effects, and thus can serve as a reference to calibrate maps of surface motion derived from InSAR.

In this paper we document how well GPS and InSAR data can

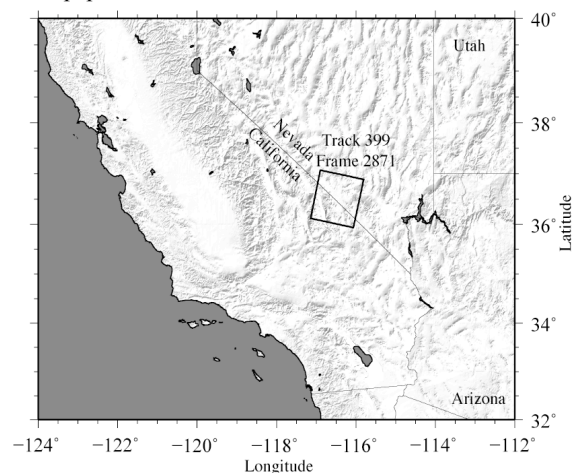


Figure 1. Map of southwest United States showing location of track 399, frame 2871 where InSAR and GPS data are obtained.

* Corresponding author

be brought into agreement by using large numbers of scenes, and aligning the results from InSAR time series analysis (Berardino et al., 2002; Li et al., 2009) that account for effects of the atmosphere to GPS solutions that are in a well-defined reference frame. This is usually accomplished by applying a transformation (e.g. a linear ramp) to the InSAR line-of-site rate maps to bring them into agreement with GPS measurements (e.g. Lundgren et al., 2009). This type of transformation is common to all geodetic techniques where the results are aligned to an external reference frame. In this case the result places the radar LOS rate maps into a global reference frame accessed with the GPS system. This exercise illustrates 1) how well InSAR time series results and GPS rates can be integrated, and 2) how well InSAR time series approach can reduce errors introduced by atmospheric effects, and 3) how well large quantities of data can reduce the effects of noise from non-secular processes. We purposefully choose an area that is challenging for detecting crustal deformation signals in order to test the technique. The western Great Basin in the vicinity of Yucca Mountain, Nevada has a very low horizontal

crustal deformation rate, ~1 mm/yr across 60 km (Wernicke et al., 2004; Hill and Blewitt, 2006). Furthermore, inside this area there are large topographic variations which include the lowest and near the highest points in the lower 48 contiguous United States. We therefore test how well the method conforms the radar LOS rate to the GPS velocity field and how well topographic effects can be removed from the LOS maps.

2. DATA

2.1 InSAR data

We used 16 ERS 1, 13 ERS 2 and 40 ENVISAT scenes from track 399 frame 2871 which straddles the Nevada/California border in the western Great Basin (Figure 1). We obtained these European Space Agency data from the UNAVCO WinSAR and GeoEarthScope archives. The acquisition times span 1992 to 2010, for a total of 17 years over which the crust progressively deformed. The dates of the scenes used are given in Table 1, and diagrams showing the interferometric pairs formed are shown in Figure 2.

2.2 Global Positioning System (GPS) data

We used data from 35 GPS stations located inside the latitude/longitude box that superscribes the radar scene (Figure 3A). These stations have 2.5–11 years of GPS observations that were used to constrain the sites rate of motion. The majority of these sites had continuous observations. This area includes the Yucca Mountain region where most sites were installed in 1999 and have over 10 years of data. Daily position solutions were obtained using the GIPSY/OASIS II software, by precise point positioning (Zumberge et al., 1997) using JPL's "flinnR" reprocessed satellite orbit and clocks. The observable model includes ocean tidal loading (including companion tides), estimation of wet zenith troposphere and two gradient parameters as a random walk process using the GMF mapping function, and antenna calibrations for ground receivers and satellite transmitters. Carrier phase ambiguity resolution was applied as part of a larger ~4,000 station global network solution using our custom Ambizap2 software (Blewitt, 2008). Solutions were transformed into the ITRF2005 reference frame and rotated so that their rates refer to motion with respect to North America. Daily solutions have common mode errors removed with respect to a North America continental-scale network. The long time series from stations in this region result in their horizontal rate uncertainties being reduced to 0.1 mm/yr or better (Davis et al., 2003), while their vertical rate uncertainties are larger by a factor between 3 and 6.

From a regional compilation of GPS velocities a continuum model of the horizontal GPS velocity field has been derived (Kreemer et al., 2009). This model velocity field interpolates the GPS rates with splines in tension to estimate the rates everywhere in the model domain. We projected these rates into the radar line-of-sight satellite geometry for comparison to the InSAR rates obtained as described below (Figure 3B). The advantage of using the strain map is that it provides stability in comparison between GPS and InSAR, since values for the interpolated velocity field are available everywhere in the scene. A disadvantage of using the strain map is that it does not incorporate information about the vertical motion of the GPS stations. However, comparison between the strain map and three-component GPS velocities, both projected into the radar line-of-sight direction, shows that they are, in this area, not different to within uncertainties (Figure 3B). Thus the

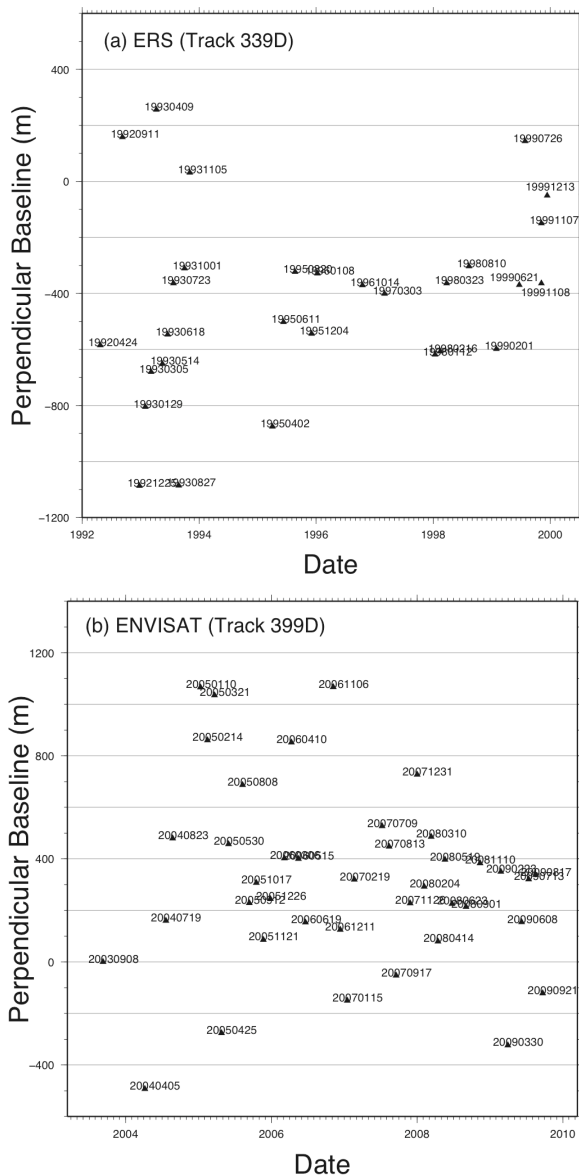


Figure 2. Baseline plot of ERS (top) and ENVISAT (bottom) scenes showing number and relative perpendicular baseline.

contribution of the vertical rates for sites in this area is not significant.

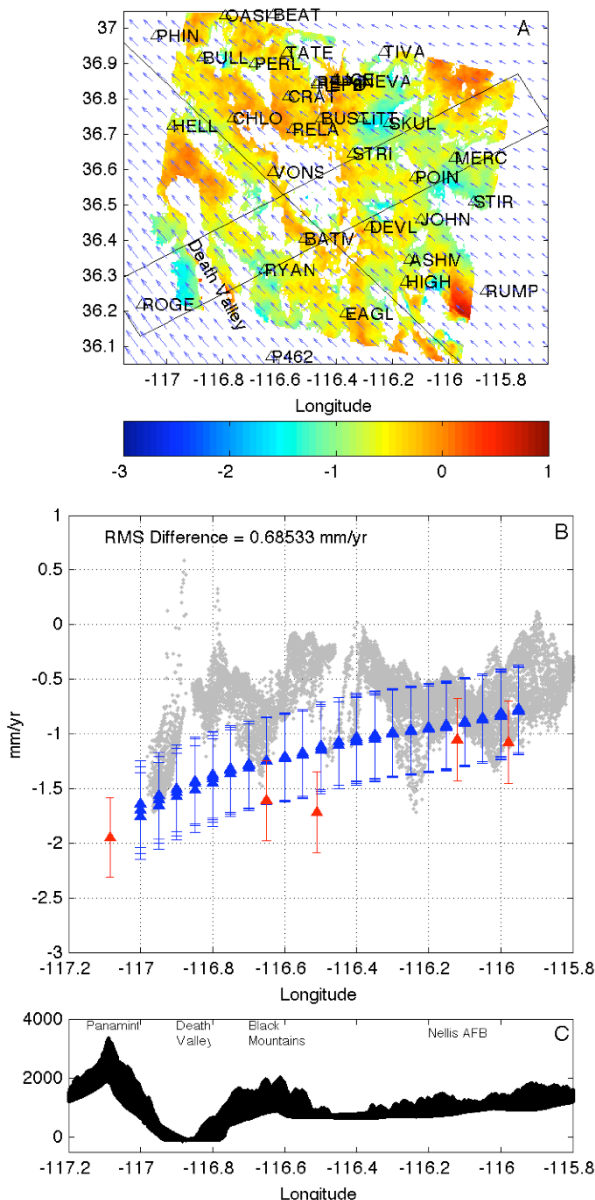


Figure 3 A) Results of time series analysis showing location of GPS sites (black triangles) and profile (black box). Blue vectors are from the horizontal GPS velocity strain map interpolation. Color scale in mm/yr. B) Results of time series analysis inside profile box (gray dots) with GPS strain map (blue triangles), and three-component GPS rates (red triangles). Uncertainties are 2-sigma, and rates and all rates in in radar LOS. C) Elevation in meters across profile.

3. ANALYSIS METHOD

From the radar scenes 146 ERS interferograms and 576 ENVISAT were formed. Coherence is generally good owing to favorable ground and atmospheric conditions. Phase unwrapping was accomplished using the SNAPHU algorithm (Chen and Zebker, 2000), which forces phase unwrapping to occur everywhere in the interferograms. To the unwrapped interferograms we applied a time series analysis that uses the

method of Li et al., (2009) which is based on the SBAS algorithm (Berardino et al., 2002; Lundgren et al., 2009). This method finds a solution for the time invariant constant motion of each pixel in the scene, plus for each scene the delays associated with atmospheric effects (i.e. an atmospheric phase screen - APS), and a component of non-linear surface motion (NSM). The APS is distinguished from the NSM by the spatial wavelength of these signal. The algorithm is applied iteratively until convergence is achieved. See Li et al., (2009) for further details. We perform the time series analysis separately for ERS and ENVISAT datasets. Since ERS and ENVISAT have roughly the same satellite-to-ground look geometry, we take a pixel-by-pixel average of the two time series analysis results to obtain LOS rate maps.

Because we are primarily interested in long-term tectonic deformation, as opposed to seasonal motions that are often observed owing to hydrological or anthropogenic influences, we apply an additional phase screen that specifically excludes areas that are especially prone to these effects. Although the time series approach should, in principal, identify such motions as APS or NSM, when the effects are large, the time series are short, or not densely sampled the cumulative effect can appear to provide a trend by aliasing a strong seasonal signal. This is the case in Death Valley, which before application of the screen, appeared to have large anomalous rates of motion in opposite directions in ERS and ENVISAT time series results. Like in Death Valley, valley bottoms in the Great Basin are composed of softer sediments or soils that experience frequent seasonal reworking owing to the actions of wind, precipitation, vegetation, livestock, etc. We construct an additional phase screen that uses the digital elevation model (DEM) to isolate regions of very flat topography. These areas are strongly correlated with the presence of younger rocks in geologic maps that have been used to develop screens based on lithology (Bürgmann et al. 2006; Hammond et al., 2006), and are nearly as effective at removing areas that experience the largest seasonal motions. Areas identified in this screen are excluded from the analysis and are shown as white areas in Figures 3A and 4A.

We assume that wherever the resulting line-of-sight velocity map is inconsistent with the GPS rates projected into radar line-of-sight, the differences are attributable to cumulative errors in the InSAR owing to long wavelength components of the atmosphere, orbit errors, etc. To correct for these errors we solve for a constant linear two-dimensional ramp based on the difference between the GPS strain map line-of-sight rates and the results of the time series analysis. This procedure effectively places the LOS rate map into the GPS reference frame, analogous to the commonly used translation and rotation transformations that are performed in reference frame alignments (e.g. Altamimi et al., 2007). Applying this adjustment reduces the misfit between InSAR and GPS substantially, as discussed below.

In a final step, we remove any residual signal that is purely an artifact of DEM error, or atmospheric signals that are correlated with topography. We solve for a simple linear model between LOS rate of motion and elevation in the DEM, and subtract the predictions of this model from the LOS motion. This step changed the RMS misfit between InSAR and GPS from 0.353 to 0.349 mm/yr, and thus had negligible effect on the final solution. This step had little effect because a DEM correction was introduced as a part of the time series analysis (Li et al., 2009), and thus there is very little residual signal that is correlated with topography (Figure 4C). Regardless of the

stage in the analysis that an elevation correction is applied, this correction has the potential to remove signal associated with the uplift of the solid earth, i.e. through tectonic extension across normal fault bounded blocks. However, the similarity between the strain map velocities (which are based on horizontal components only) projected into the satellite LOS and the full three-component rates at the GPS sites projected into LOS (e.g. Figure 4B), suggests that vertical motions are too small to be a significant contribution in this case.

To estimate the LOS rate from the InSAR we averaged the LOS rates around each point in the GPS strain map inside a circle of radius 3 km. This averages the InSAR LOS rates over an area comparable to the spacing in the velocity interpolation in the strain map (Figures 3B and 4B), and effectively smooths the radar LOS rate map for the purpose of comparison to GPS rates.

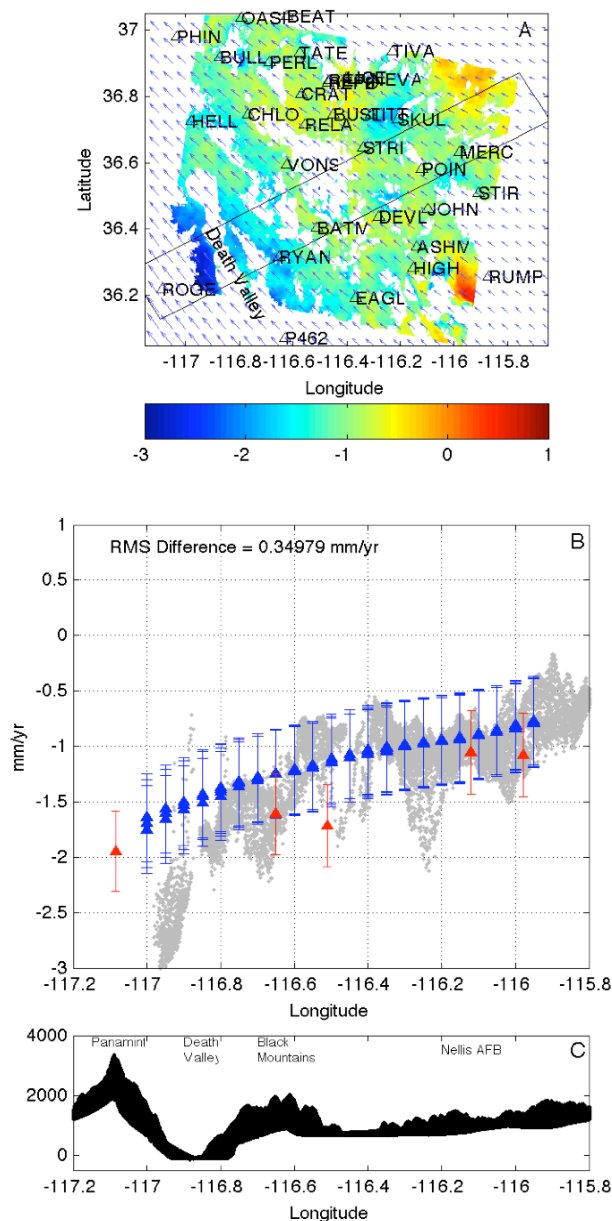


Figure 4. Same as Figure 3, except that a ramp aligning the radar LOS map to the GPS, and an additional model correcting for topographic effects have been removed.

4. RESULTS AND CONCLUSIONS

Before correcting for inconsistency between GPS and InSAR LOS rates, the root-mean-square (RMS) misfit between GPS strain map and InSAR was 0.69 mm/yr across the entire scene (Figure 2A). After applying the ramp to correct for the inconsistency between GPS strain map and InSAR, this RMS misfit decreases to 0.35 mm/yr. The misfit between GPS LOS rates at the stations, and the values at the same locations in the GPS strain map (i.e. the difference between GPS data and interpolated model obtained from GPS) is 0.31 mm/yr. Thus the misfit between InSAR LOS rates and GPS is only slightly larger than the difference between GPS models and data.

It is important to recognize that the scale on the vertical axis in Figures 3B and 4B is in units of mm/yr, and thus the scatter of the InSAR LOS motion occupies a band about 0.5–0.7 mm/yr wide. This is a factor of 2–4 smaller than the scatter in the radar LOS rates published in some recent studies (e.g. Fialko, 2006; Lundgren, 2009) which reported uncertainties on the order of 1–2 mm/yr based on similar data and methods.

The implication of this analysis is that when long-term velocities are estimated with InSAR using large numbers of scenes acquired over many years (>17 years time span in this case), the uncertainties are similar to those in the GPS data. This suggests that if a deformation signal exists in the solid earth with a geographic wavelength smaller than the GPS spacing (e.g. a creeping fault) it could be detected if its amplitude is larger than the level of noise in the InSAR (e.g. >0.35 mm/yr), even if it were missed by the GPS network. It may be the case that the actual Earth motion is similar to the LOS rates shown in Figure 4B, but that our GPS networks do not have sufficient geographic density to image short wavelength variations in the geodetic velocity field.

Our results bode well for the utility of present and future satellite missions (e.g. ALOS/PALSAR, Sentinel, DESDynI) that promise to acquire long time series of radar images for two-pass interferometry. The DESDynI mission (a planned NASA L-band mission) will have shorter repeat time, and thus increase the amount of data collected of a similar number of years, or conversely will decrease the number of years it takes to achieve a similar degree of precision. The results also bode well for more general applications to geohazards than what we expect in our test area. An important focus related to geohazards is on detecting transient signals in the velocity field in order to make the methodology applicable for monitoring of volcanoes, landslide-prone areas, and potential subsidence.

REFERENCES

- Altamimi, Z., X. Collilieux, J. Legrand, B. Garayt, and C. Boucher (2007), ITRF2005: A new release of the International Terrestrial Reference Frame based on time series of station parameters and Earth Observation Parameters, *J. Geophys. Res.*, 112, B09401, doi:10.1029/2007JB004949.
- Bennett, R. A., B. P. Wernicke, N. A. Niemi, A. M. Friedrich, and J. L. Davis (2003), Contemporary strain rates in the northern Basin and Range province from GPS data, *Tectonics*, 22, 1008, doi:10.1029/2001TC001355.
- Berardino, P., G. Fornaro, R. Lanari, and E. Sansosti (2002), A new algorithm for surface deformation monitoring based on small baseline differential SAR Interferograms, *IEEE Trans.*

Geos. Rem. Sens., 40, 11, 2375-2383.

Blewitt, G. (2008), Fixed-Point theorems of GPS carrier phase ambiguity resolution and their application to massive network processing: "Ambizap", *J. Geophys. Res.*, 113, B12410, doi:10.1029/2008JB005736.

Blewitt, G., W.C. Hammond, and C. Kreemer (2009). Geodetic observation of contemporary strain in the northern Walker Lane:1, Semi-permanent GPS strategy. *Late Cenozoic Structure and Evolution of the Great Basin – Sierra Nevada Transition*, Vol. 447, pp. 1-15, Geological Society of America. doi: 10.1130/2009.2447(01).

Bürgmann, R., G. Hilley, A. Ferretti, and F. Novali (2006), Resolving vertical tectonics in the San Francisco Bay Area from permanent scatterer InSAR and GPS analysis, *Geology*, 34, 3, 221-224.

Chen, C. W., and H. A. Zebker (2000), Network approaches to two-dimensional phase unwrapping: intractability and two new algorithms, *J. Opt. Soc. Amer. A-Opt. Image Sci. Vis.*, 17, 3, 401-414.

Davis, J. L., R. A. Bennett, and B. P. Wernicke (2003), Assessment of GPS velocity accuracy for the Basin and Range Geodetic Network (BARGEN), *Geophys. Res. Lett.*, 30, 7, 61-64.

Fialko, Y. (2006), Interseismic strain accumulation and the earthquake potential on the southern San Andreas fault system, *Nature*, 441, 7096, 968-971.

Hammond, W. C., Z. Li, H.-P. Plag, G. Blewitt, and C. Kreemer (2006), Results of InSAR and GPS measurement of tectonic deformation near the Eastern California Shear Zone and Yucca Mountain, Nevada, *Eos Trans. AGU Fall Meet. Suppl.*, 87(52).

Hammond, W. C., and W. Thatcher (2007), Crustal Deformation across the Sierra Nevada, Northern Walker Lane, Basin and Range Transition, western United States Measured with GPS, 2000-2004, *J. Geophys. Res.*, 112, B05411, doi:10.1029/2006JB004625.

Hill, E., and G. Blewitt (2006), Testing for fault activity at Yucca Mountain, Nevada, using independent GPS results from the BARGEN network, *Geophys. Res. Lett.*, 33, L14302, doi:10.1029/2006GL026140.

Kreemer, C., G. Blewitt, and W. C. Hammond (2009), Geodetic constraints on contemporary deformation in the northern Walker Lane: 2, velocity and tensor strain rate analysis, *Late Cenozoic Structure and Evolution of the Great Basin – Sierra Nevada Transition*, Special Paper 447, doi: 10.1130/2009.2447(02).

Li, Z. H., E. J. Fielding, and P. Cross (2009), Integration of InSAR Time-Series Analysis and Water-Vapor Correction for Mapping Postseismic Motion After the 2003 Bam (Iran) Earthquake, *IEEE Trans. Geos. Rem. Sens.*, 47, 9, 3220-3230.

Lundgren, P., E. A. Hetland, Z. Liu, and E. J. Fielding (2009), Southern San Andreas-San Jacinto fault system slip rates estimated from earthquake cycle models constrained by GPS and interferometric synthetic aperture radar observations, *J. Geophys. Res.*, 114, B02403, doi:10.1029/2008JB005996.

Wernicke, B. P., J. L. Davis, R. A. Bennett, J. E. Normandeau, A. M. Friedrich, and N. A. Niemi (2004), Tectonic Implications of a dense continuous GPS velocity field at Yucca Mountain, Nevada, *J. Geophys. Res.*, 109, B12404.

Wesnousky, S. G. (2005), Active faulting in the Walker Lane, *Tectonics*, 24, TC3009, doi:10.1029/2004TC001645.

Zebker, H., M. Williams, D. Sandwell, and A. Donnellan (2010), Op - Ed - InSAR; An essential component of EarthScope, *inSights - The EarthScope Newsletter*, Spring 2010.

Zumberge, J. F., M. B. Heflin, D. C. Jefferson, M. M. Watkins, and F. H. Webb (1997), Precise point positioning for the efficient and robust analysis of GPS data from large networks, *J. Geophys. Res.*, 102, B3, 5005-5017.

ACKNOWLEDGEMENTS

This research is made possible with support from the NASA EarthScope Geodetic Imaging project NNX09AD24G, and the NSF EarthScope project 0844389. Part of this work was carried out in the University of Glasgow, which was supported by the Natural Environmental Research Council (NERC) through the GAS project (Ref: NE/H001085/1) and was also supported in part by a 863 Project (ID: 2009AA12Z317). We thank UNAVCO, Inc. for providing data used in this study via the WinSAR and GeoEarthScope data archives, and IGS for global GPS data. We used the ROI_PAC, Gamma and GMT softwares for various components of this analysis and presentation.